Neutrino-Induced Coherent π^+ Production in C, CH, Fe, and Pb at $\langle E_\nu \rangle \sim 6$ GeV

M. A. Ramírez [1,2] S. Akhter,[3] Z. Ahmad Dar,[4,3] F. Akbar,[3] V. Ansari,[3] M. V. Ascencio,[5,*] M. Sajjad Athar,[3] A. Bashyal,[6,†]
L. Bellantoni,[7] A. Bercellie,[8] M. Betancourt,[7] A. Bodek,[8] J. L. Bonilla,[2] A. Bravar,[9] H. Budd,[8] G. Caceres,[10,‡] T. Cai,[8]
G. A. Díaz,[8] H. da Motta,[10] S. A. Dytman,[11] J. Felix,[2] L. Fields,[12] A. Filkins,[4] R. Fine,[8,§] H. Gallagher,[13] A. Ghosh,[14,10]
S. M. Gilligan,[6] R. Gran,[15] E. Granados,[2] D. A. Harris,[16,7] S. Henry,[8] D. Jena,[7] S. Jena,[17] J. Kleykamp,[8,‖] A. Klustová,[18]
M. Kordosky,[4] D. Last,[1] A. Lozano,[10] X.-G. Lu,[19,20] E. Maher,[21] S. Manly,[8] W. A. Mann,[13] C. Mauger,[1] K. S. McFarland,[8]
B. Messerly,[11,¶] J. Miller,[14] O. Moreno,[4,2] J. G. Morfín,[7] D. Naples,[11] J. K. Nelson,[4] C. Nguyen,[22] A. Olivier,[8] V. Paolone,[11]
G. N. Perdue,[7,8] K.-J. Plows,[20] R. D. Ransome,[23] D. Ruterbories,[8] H. Schellman,[6] H. Su,[11] M. Sultana,[8] V. S. Syrotenko,[13]
E. Valencia,[4,2] N. H. Vaughan,[6] A. V. Waldron,[18] B. Yaeggy,[14,**] and L. Zazueta[4]

(The MINERvA Collaboration)

[1]*Department of Physics and Astronomy, University of Pennsylvania, Philadelphia, Pennsylvania 19104, USA*
[2]*Campus León y Campus Guanajuato, Universidad de Guanajuato,*
Lascurain de Retana No. 5, Colonia Centro, Guanajuato 36000, Guanajuato, Mexico
[3]*Department of Physics, Aligarh Muslim University, Aligarh, Uttar Pradesh 202002, India*
[4]*Department of Physics, William & Mary, Williamsburg, Virginia 23187, USA*
[5]*Sección Física, Departamento de Ciencias, Pontificia Universidad Católica del Perú, Apartado 1761, Lima, Peru*
[6]*Department of Physics, Oregon State University, Corvallis, Oregon 97331, USA*
[7]*Fermi National Accelerator Laboratory, Batavia, Illinois 60510, USA*
[8]*Department of Physics and Astronomy, University of Rochester, Rochester, New York 14627, USA*
[9]*University of Geneva, 1211 Geneva 4, Switzerland*
[10]*Centro Brasileiro de Pesquisas Físicas, Rua Dr. Xavier Sigaud 150, Urca, Rio de Janeiro, Rio de Janeiro, 22290-180, Brazil*
[11]*Department of Physics and Astronomy, University of Pittsburgh, Pittsburgh, Pennsylvania 15260, USA*
[12]*Department of Physics, University of Notre Dame, Notre Dame, Indiana 46556, USA*
[13]*Physics Department, Tufts University, Medford, Massachusetts 02155, USA*
[14]*Departamento de Física, Universidad Técnica Federico Santa María, Avenida España 1680 Casilla 110-V, Valparaíso, Chile*
[15]*Department of Physics, University of Minnesota—Duluth, Duluth, Minnesota 55812, USA*
[16]*York University, Department of Physics and Astronomy, Toronto, Ontario, M3J 1P3, Canada*
[17]*Department of Physical Sciences, IISER Mohali, Knowledge City, SAS Nagar, Mohali - 140306, Punjab, India*
[18]*The Blackett Laboratory, Imperial College London, London SW7 2BW, United Kingdom*
[19]*Department of Physics, University of Warwick, Coventry, CV4 7AL, United Kingdom*
[20]*Oxford University, Department of Physics, Oxford, OX1 3PJ, United Kingdom*
[21]*Massachusetts College of Liberal Arts, 375 Church Street, North Adams, Massachusetts 01247, USA*
[22]*University of Florida, Department of Physics, Gainesville, Florida 32611, USA*
[23]*Rutgers, The State University of New Jersey, Piscataway, New Jersey 08854, USA*

MINERvA has measured the ν_μ-induced coherent π^+ cross section simultaneously in hydrocarbon (CH), graphite (C), iron (Fe), and lead (Pb) targets using neutrinos from 2 to 20 GeV. The measurements exceed the predictions of the Rein-Sehgal and Berger-Sehgal PCAC based models at multi-GeV ν_μ energies and at produced π^+ energies and angles, $E_\pi > 1$ GeV and $\theta_\pi < 10°$. Measurements of the cross-section ratios of Fe and Pb relative to CH reveal the effective A scaling to increase from an approximate $A^{1/3}$ scaling at few GeV to an $A^{2/3}$ scaling for $E_\nu > 10$ GeV.

In neutrino-induced coherent pion production the nucleons in the nucleus recoil in phase under the impact of an incident neutrino. The nucleus remains in its initial quantum state and recoils with an energy below the detection threshold of most neutrino detectors. A π meson and a lepton are created, both with relatively small angles with respect to the incoming neutrino. Both charged (CC) and neutral current (NC) interactions can occur, induced by a neutrino or antineutrino of any flavor, according to $\nu_l + A \rightarrow l + \pi + A$, where ν_l is a neutrino of flavor l, A is the nucleus, and l and π, a lepton and a pion of the proper charge, respectively. The four-momentum transfer to the nucleus,

$$|t| = |(p_\nu - p_l - p_\pi)^2|$$
$$\approx \left(\sum_{i=l,\pi} \mathbf{p}_i^T\right)^2 + \left(\sum_{i=l,\pi} E_i - p_i^L\right)^2, \quad (1)$$

must be between $|t_{\min}| \simeq [(Q^2 + m_\pi^2)/2E_\pi]^2$ [1], and $|t_{\max}| = 1/R_N^2$ [2] for the interaction to happen, where p_ν, p_l, and p_π are the neutrino, lepton, and pion four-momenta, respectively; $\mathbf{p}^T$ and p^L are the lepton's or pion's transverse and longitudinal momenta, respectively; E is the lepton's or pion's total energy, Q^2 is the square of the four-momentum transferred by the neutrino, m_π is the pion mass, and R_N is the nuclear radius.

Historically, most experiments [2–17] used the Rein-Sehgal model (R-S) [18] to simulate coherent π production. It is based on Adler's partially conserved axial current (PCAC) theorem [19], which relates the neutrino-nucleus inelastic cross section to the pion-nucleus elastic cross section, assuming the incoming neutrino and the outgoing lepton are parallel (when $Q^2 = 0$), and neglecting the lepton mass. The CC channel differential cross section is

$$\left.\frac{d^3\sigma_{coh}^{CC}}{dQ^2 dy d|t|}\right|_{Q^2=0} = \frac{G_F^2 f_\pi^2}{2\pi^2} \frac{1-y}{y} \frac{d\sigma^{\pi^\pm A}}{d|t|}, \quad (2)$$

where $y = \nu/E_\nu = (E_\nu - E_\mu)/E_\nu \approx E_\pi/E_\nu$, f_π^2 is the pion decay constant, E_ν is the neutrino energy, and $d\sigma^{\pi^\pm A}/d|t|$ is the pion-nucleus elastic cross section. The model extrapolates Eq. (2) to $Q^2 > 0$ with a form factor $[m_A^2/(m_A^2 + Q^2)]^2$, where $m_A \approx 1$ GeV is the axial-vector mass.

CC coherent pion production is an important background for CC quasielastic interactions in ν_μ-disappearance measurements [20], when the π^+ is misreconstructed as a proton. It is also a significant fraction of MINERvA's own CC1π^+ sample [21]. Both are very valuable for upcoming neutrino oscillation analyses in the few-GeV region [22,23].

By using $|t|$ to isolate signal-like events, MINERvA was the first experiment to observe the CC coherent $\pi^\pm$ in that energy region, using ν_μ and $\bar{\nu}_\mu$ beams on a hydrocarbon

(CH) target [24,25]. These and two later publications [26,27] used an improved version of the R-S model that includes the lepton mass [28,29].

Prior to this work, all published results on coherent pion production used a single target with mass number $A \leq 40$ ($A \leq 80$ for NC) [2–17,24–27]. Compared to the previous MINERvA measurement, the present work uses data from a more energetic and more intense beam [30], and from a longer exposure, representing an increase of the protons on target (POT), from $\sim 3 \times 10^{20}$ to $\sim 10.5 \times 10^{20}$. This Letter presents measurements carried out simultaneously on four different samples: hydrocarbon (CH), graphite (C), steel (Fe), and lead (Pb). Absolute cross sections and ratios to scintillator (CH) are reported for nuclei with a wide range of A values: 12, 56, and 207.

These measurements are obtained using the NuMI beam line at the Fermi National Accelerator Laboratory [31] where 120-GeV protons colliding on a graphite target, create hadrons that are focused using a pair of magnetic horns, and sent to a decay pipe where they create a beam of muon-neutrinos, with $\langle E_\nu \rangle \sim 6.0$ GeV [30], made of $\sim 95\% \nu_\mu$, and $\sim 5\%$ of $\bar{\nu}_\mu$, ν_e, and $\bar{\nu}_e$ [32]. The neutrino beam is simulated with a GEANT4 model [33,34].

The MINERvA detector consists of an inner detector made of an upstream "nuclear target" and a downstream "tracker" region, and an outer detector composed of electromagnetic (ECAL) and hadronic (HCAL) calorimeters [35]. The nuclear target region is ~ 1.4 m long with five different passive materials: solid C, Fe, and Pb; and liquid He and H_2O, all installed in seven targets. Following the beam direction, solid targets are labeled from 1 to 5. Targets 1, 2, and 5 had segments of Fe and Pb, and thickness of ~ 2.6 cm in targets 1 and 2, and ~ 1.3 cm in target 5. Target 3 had C, Fe, and Pb segments, with thickness of ~ 7.6, ~ 2.9, and ~ 2.6 cm, respectively. Target 4 was made of Pb with a thickness of ~ 0.8 cm. Eight planes of tracking plastic scintillator (CH) were placed between the targets (only four between targets 4 and 5). Different target positions and thicknesses tried to equalize mass, acceptance, and particle containment; maximize event rates, vertex and track resolution; and minimize the energy threshold of particles exiting the passive materials. The tracker region is ~ 2.7 m long and made of 120 scintillator planes. Planes consist of 127 triangular prism scintillator strips with 33-mm base, 17-mm height, and varying length to form a hexagonal plane. Planes are rotated by 60° with respect to adjacent ones, enabling three-dimensional reconstruction. The detector's single hit position resolution is ~ 3 mm and the time resolution is 3 ns [35]. The ECAL surrounds the inner detector, and the HCAL surrounds the ECAL. The former (latter) consists of planes of lead (iron) and scintillator to contain and track electromagnetically (strongly) interacting particles. Located 2 m downstream of MINERvA, the MINOS near detector [36,37] served as a magnetized spectrometer to determine muon charge and momentum.

The signal process is CC coherent interactions on C, Fe, and Pb, induced by a ν_μ from 2 to 20 GeV. Events with pion angle larger than $70°$ cannot be tracked and have zero efficiency. Events in the nuclear target (tracker) region with muon angle larger than $13°$ have an efficiency of $\sim1\%$ ($\sim4\%$) due to MINOS acceptance. The percentage of simulated signal events in these categories is $\sim5\%$ for CH and C, and $\sim2\%$ for Fe and Pb.

Neutrino interactions are simulated using a modified version of the GENIE event generator v2.12.6 [38,39]. The signal's cross section is given by the R-S model with the lepton mass correction. Background processes (Fig. 1) in increasing hadronic invariant mass W, are CC quasielastic (QE), correlated pairs of nucleons (2p2h), resonant π^+ production (non-QE, $W < 1.4$ or RES), inelastic scattering ($1.4 < W < 2.0$ or INE) and deep inelastic scattering ($W > 2.0$ or DIS). Quasielastic scattering is simulated using the Llewellyn-Smith model [40] with an axial-vector form factor from a z expansion fit to deuterium data [41] and a correction from the Valencia random phase approximation (RPA) [42]. The $2p2h$ process is simulated with the Valencia model [43–45] and modified according to a "low recoil" fit by MINERvA [46]. Resonant pion production uses the Rein-Sehgal model [47] with its normalization increased 15% based on fits from a deuterium data analysis [48], plus an additional *ad hoc* suppression for $Q^2 < 0.7$ $[\text{GeV}/c]^2$ due to collective nuclear effects [49]. Inelastic interactions use a tuned model of discrete baryon resonances [47], and the Bodek-Yang model for the transition region to DIS, as well as nonresonant pion production across the full W range [50], that was reduced by 43% based on a tune to the same deuterium data [48]. These tunes to GENIE are labeled as the MINERvA tune v4.4.1 [51].

Final state particles coming from the GENIE simulation are propagated through the detector using a GEANT4
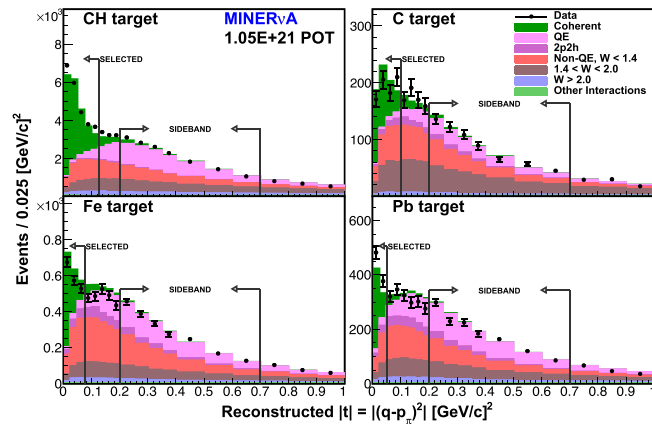

FIG. 1. Reconstructed $|t|$ distributions after E_{vtx} cut and background tuning: CH, C, Fe, and Pb, in reading order. Regions in between arrows are the sidebands for background tuning. Events to the left of the lower-$|t|$ arrow are selected.

simulation of the detector's geometry and material composition, light yield and energy deposition of the particles in the scintillator, and their hadronic and electromagnetic interactions [35]. The detector's energy scale was established by making sure that simulated through-going muons agreed with data in both light yield and reconstructed energy deposition. The detector's simulated response to different particles is validated in a test beam measurement [52], and the effects of accidental activity, electronics charge, and time resolution were also included [35].

Scintillator strips with deposited energy greater than 1 MeV are grouped per plane according to their position and time, into "clusters." These are grouped with clusters in adjacent planes to form tracks. Backwards-projected tracks find interaction vertices. Angles are measured between the simulated beam direction and the direction of the track in its first planes downstream of the vertex.

This analysis isolates events with two tracks from a common vertex. The reconstructed momentum of the muon candidate is the addition of the momentum determined by range inside MINERvA plus its momentum determined by range or curvature inside MINOS. The pion candidate has to be fully contained inside MINERvA, so $|t|$ can be measured. The pion total energy is reconstructed calorimetrically from all the energy not associated with the muon, given the assumption $E_\nu \approx E_\pi + E_\mu$ from Eq. (1), where E_μ is the muon's total energy.

The reconstructed interaction vertex is defined as the upstream end of the muon track, and it is required to be inside the fiducial volume under study. The CH fiducial volume is 108 planes long (~2.4 m) centered in the tracker region with the area of a 0.85-m apothem hexagon [53]. The fiducial volume in the passive targets, is the area times the thickness of the segment of interest. For the passive materials, the vertex is projected into the z center of the target, where the (x, y) coordinate determines the segment (material). Events from different targets but the same material are combined into a single sample.

The reconstructed neutrino energy must be between 2 and 20 GeV to remove events with misreconstructed muon energy [34]. To reject protons from quasielastic and resonance production backgrounds, dE/dx-based χ^2 compared to pion and proton hypotheses of the pion candidate track are built. A log likelihood ratio [54] between the hypotheses removes (keeps) $\sim70\%$ ($\sim87\%$) of protons (pions) according to the simulation.

The energy of the vertex region (E_{vtx}), defined as a 200-mm radius, 7-plane height cylinder centered at the interaction vertex, must be consistent with the energy deposited by one minimum-ionizing charged pion and one muon. The E_{vtx} distribution of simulated signal events is fit to a Gaussian function, and events within $\pm1\sigma$ of the mean are selected. Because of different target thickness, $\langle E_{vtx}\rangle$ is target dependent, varying from ~60 to ~95 MeV. This cut removes (keeps) $\sim86\%$ ($\sim60\%$) of the background (signal).

Because of their proximity to tracking scintillator planes, the C, Fe, and Pb samples have contamination from events occurring in the scintillator upstream and downstream of the passive material. These events are considered background, and are tuned using the plastic regions between passive targets as sidebands. There is an "upstream" and a "downstream" plastic sideband for each passive material. The tuned plastic backgrounds represent $\sim 13\%$, $\sim 14\%$, and $\sim 21\%$ of the C, Fe, and Pb selected samples, respectively.

After removing events with high E_{vtx}, and subtracting the plastic background, all samples in Fig. 1 show a signal dominance at low $|t|$. For heavier nuclei, the signal shrinks to a lower $|t|$ region as R_N increases. The C distribution has a significant excess of RES and INE events from ~ 0.025 to ~ 0.5 $[\mathrm{GeV/c}]^2$ compared to CH, despite both being interactions on carbon. This is due to the ~ 7.6-cm thickness of the C segment, where one or more pions from those backgrounds are absorbed inside the passive material, which allows the event to pass the E_{vtx} cut.

A high $|t|$ sideband ($0.2 < |t| < 0.7$ $[\mathrm{GeV/c}]^2$) is used to tune the QE, RES (Non-QE, $W < 1.4$), INE ($1.4 < W < 2.0$), and DIS ($W > 2.0$) backgrounds. Because of their small content, "coherent" and "other interactions" (NC-, $\bar{\nu}_\mu$-, or $\overset{(-)}{\nu}_e$-induced) are not tuned, and $2p2h$ is considered QE during the tuning. Because the C target has limited statistics, two modifications were made to the fit for that target only: RES and INE were combined, and the QE and DIS scale factors were replaced by their CH counterparts. The scale factors for each of the backgrounds are in the Supplemental Material [55].

Events with $|t| < (0.1, 0.125, 0.075, \text{and } 0.05)$ $[\mathrm{GeV/c}]^2$ were selected for C, CH, Fe, and Pb, respectively. More than 99% of GENIE true signal events are below those cuts. After the $|t|$ cut and background subtraction, there are 14855 ± 433 CH, 303 ± 41 C, 726 ± 89 Fe, and 492 ± 41 Pb candidate events.

An iterative unfolding approach [56] was used to correct the background-subtracted distributions for resolution effects. The unfolded distributions were then efficiency corrected. The cross sections were extracted according to the expression $\sigma = N^{\mathrm{DATA\ eff}}/(\Phi T)$, where $N^{\mathrm{DATA\ eff}}$ is the background-subtracted, unfolded, and efficiency-corrected data, Φ is the incident neutrino flux, and T the number of C, Fe, or Pb nuclei. The largest sources of inefficiency come predominantly from well-understood random processes, which supports the assumption that the nondetected events have the same relative background composition.

The extracted cross sections are compared to the R-S model (GENIE v2.12.6) and to the Berger-Sehgal (B-S) model (GENIE v3.0.6) [57–59]. The latter is also PCAC-based, and also includes the muon mass correction, but uses pion-carbon data [1] to model the elastic pion-nucleus cross section, instead of pion-deuterium data as the R-S model.
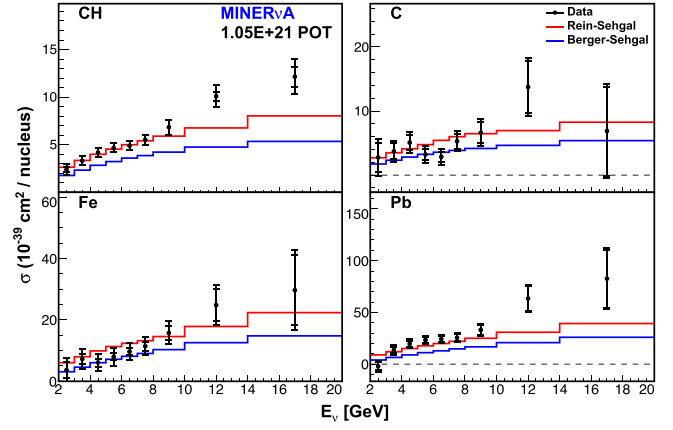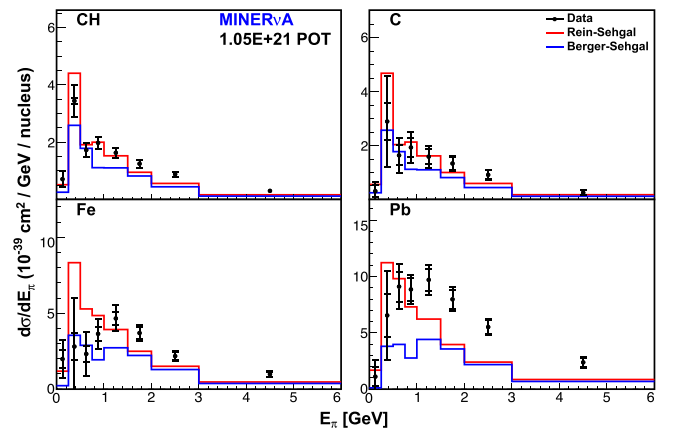

FIG. 2. Total cross sections as a function of E_ν: CH, C, Fe, and Pb, in reading order. Data are compared to the R-S (red) and B-S (blue) models.

Figure 2 shows the total cross section as a function of E_ν, with the flux integrated per bin, where both models underpredict the reaction rate at high neutrino energies in the four materials. Inner (outer) error bars are the statistical (statistical + systematic) uncertainties. The differential cross sections with respect to E_π and θ_π, are flux averaged from $2 < E_\nu < 20$ GeV. In $d\sigma/dE_\pi$ (Fig. 3) there is a clear disagreement between the models and the data of the two heavier nuclei, for low (high) E_π in iron (lead). Figure 4 shows that the models also underpredict the $d\sigma/d\theta_\pi$ cross section at very forward angles in all materials. Notably, forward pion production in the heavier nuclei is enhanced relative to scattering on carbon, where for lead, the cross section becomes negligible for $\theta_\pi > 30°$.

The simultaneous neutrino exposure of the various targets enables precise measurement of cross section ratios thanks to the same beam configuration in all targets at any given time. Figure 5 shows the cross section ratios as a function of E_ν: σ_C/σ_{CH}, σ_{Fe}/σ_{CH}, and σ_{Pb}/σ_{CH}.

FIG. 3. Differential cross sections as a function of E_π: CH, C, Fe, and Pb, in reading order. Data are compared to the R-S (red) and B-S (blue) models.
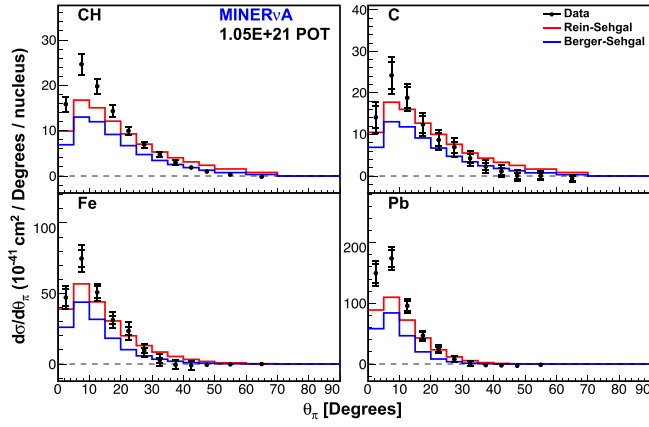
FIG. 4. Differential cross sections as function of θ_π: CH, C, Fe, and Pb, in reading order. Data are compared to the R-S (red) and B-S (blue) models.

As expected, the former is consistent with unity [60]. The CH cross sections used to calculate the ratios, were reweighted to use a flux that matched the flux used to calculate the C, Fe, or Pb cross sections [21].

The R-S and B-S models predict a scaling of the cross-section with respect to the mass number A and practically energy independent (horizontal dashed lines in Fig. 5), $\sim A^{1/3}$ [18,61] and $\sim A^{2/3}$ [3,62], respectively. The PCAC-based Belkov-Kopeliovich (B-K) model predicts a scaling close to $A^{1/3}$ at low pion energy but close to $A^{2/3}$ at high pion energy [63,64]. In terms of neutrino energy, the B-K model predicts a scaling of $\sim A^{1/3}$ ($\sim A^{2/3}$) at neutrino energies below (above) ~ 10 GeV [65].

The measured $\sigma_{\text{Fe}}/\sigma_{\text{CH}}$ resembles the trend predicted by B-K, where below ~ 8 GeV there is a clear agreement with the $A^{1/3}$ scaling, and a better agreement with the $A^{2/3}$ scaling above ~ 10 GeV, with a constant increase in
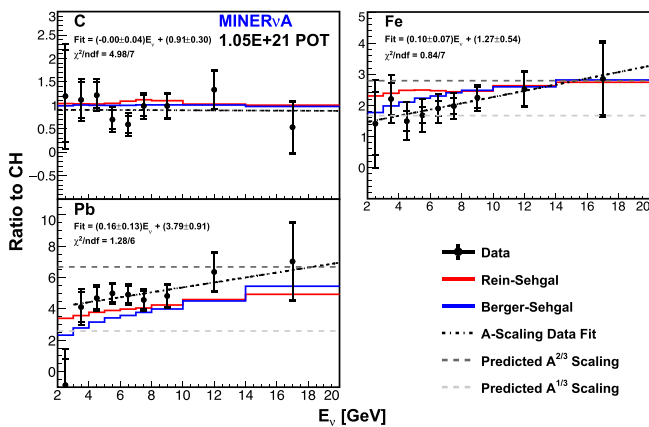

FIG. 5. Cross section ratios as a function of E_ν: $\sigma_{\text{C}}/\sigma_{\text{CH}}$, $\sigma_{\text{Fe}}/\sigma_{\text{CH}}$, and $\sigma_{\text{Pb}}/\sigma_{\text{CH}}$, in reading order. The upper (lower) dashed line is the ratio predicted by an $A^{2/3}$ ($A^{1/3}$) scaling. The slope is the best A-scaling fit. The 2–3 GeV bin is not included in the $\sigma_{\text{Pb}}/\sigma_{\text{CH}}$ fit due to the null cross section in lead in that bin (Fig. 2).

between. A similar trend occurs for the measured $\sigma_{\text{Pb}}/\sigma_{\text{CH}}$ but with an A-scaling larger than predicted below 10 GeV.

The statistical uncertainty of the total cross section dominates in the three passive materials (Fig. 6). The largest systematic uncertainties are related to the detector's geometry and particles interacting in it (Detector Model), like the muon energy deposition in MINERvA and MINOS [66]. Uncertainties associated with the "interaction model," come from GENIE and the uncertainties from the MINERvA tune v.4.4.1. The "physics sideband" is the uncertainty on the backgrounds scale factors, plus a "per-bin" uncertainty covering for the remaining disagreement between data and the simulation in the high $|t|$ sideband.

The "flux" uncertainty comes from the uncertainty on the beam line parameters, and hadron interactions [34]. It was further constrained from 7.6% to 3.9% using a neutrino-electron scattering measurement [67].

Other sources of uncertainty are the discrepancy in the detector mass; modifications to the QE-like background (low recoil and RPA); low Q^2 suppression of resonant pion production; and the uncertainty on the plastic background scale factors (plastic sideband). They contribute less than $\sim 5\%$ ($\sim 15\%$) to the total cross section uncertainty in CH (C, Fe, and Pb). The CH sample provides the most precise measurement of the interaction so far, reducing the total uncertainty from $\sim 25\%$ to $\sim 15\%$ compared to the previous MINERvA measurement [25]. Cross section ratios have a further reduction of some systematic uncertainties, in particular the flux, reduced by $\sim 75\%$ of itself (Fig. 6).

The measurements in this Letter represent the first simultaneous measurement of the interaction in multiple materials and the first measurement in nuclei with $A > 40$ (^{56}Fe and ^{207}Pb), from which cross section ratios with respect to CH are measured. The data indicates that the R-S and B-S PCAC models do not accurately describe the angular dependence on θ_π, the energy dependence on E_π, or
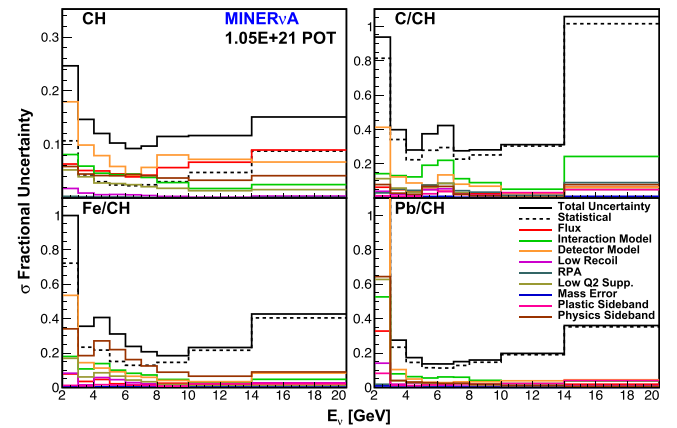

FIG. 6. Uncertainties in the total cross section as a function of E_ν: CH, C/CH, Fe/CH, and Pb/CH, in reading order. The systematic uncertainties are described in the text.

the *A* dependence. While the σ_{Fe}/σ_{CH} qualitatively agrees with the B-K model's energy-dependent *A* scaling, σ_{Pb}/σ_{CH} does not, at least at low E_ν.

The estimate of the cross sections *A* scaling provided in this Letter could be used to extrapolate to materials where measurements do not exist or the statistics are limited, like H_2O for Hyper-K or Ar for DUNE. For the latter, pion production will make up around three quarters of the detected neutrino-induced events.

[*]Present address: Iowa State University, Ames, Iowa 50011, USA.

[†]Present address: High Energy Physics/Center for Computational Excellence Department, Argonne National Lab, 9700 S Cass Ave., Lemont, Illinois 60439, USA.

[‡]Present address: Department of Physics and Astronomy, University of California at Davis, Davis, California 95616, USA.

[§]Present address: Los Alamos National Laboratory, Los Alamos, New Mexico 87545, USA.

[‖]Present address: Department of Physics and Astronomy, University of Mississippi, Oxford, Mississippi 38677, USA.

[¶]Present address: University of Minnesota, Minneapolis, Minnesota 55455, USA.

[**]Present address: Department of Physics, University of Cincinnati, Cincinnati, Ohio 45221, USA.

[1] E. A. Paschos, A. Kartavtsev, and G. J. Gounaris, Coherent pion production by neutrino scattering off nuclei, Phys. Rev. D **74**, 054007 (2006).

[2] P. Vilain *et al.* (CHARM II Collaboration), Coherent single charged pion production by neutrinos, Phys. Lett. B **313**, 267 (1993).

[3] H. Faissner, E. Frenzel, M. Grimm, T. Hansl-Kozanecka, D. Hoffmann, E. Radermacher, D. Rein, H. Reithler, U. Samm, L. M. Sehgal *et al.* (Achen-Padova Collaboration), Observation of neutrino and anti-neutrino induced coherent neutral pion production off ^{27}Al, Phys. Lett. **125B**, 230 (1983).

[4] E. Isiksal, D. Rein, and J. G. Morfin, Evidence for Neutrino and Anti-Neutrino Induced Coherent π^0 Production, Phys. Rev. Lett. **52**, 1096 (1984).

[5] P. Marage *et al.* (WA59 Collaboration), Observation of coherent diffractive charged current interactions of anti-neutrinos on neon nuclei, Phys. Lett. **140B**, 137 (1984).

[6] F. Bergsma *et al.* (CHARM Collaboration), Measurement of the cross-section of coherent π^0 production by muon neutrino and anti-neutrino neutral current interactions on nuclei, Phys. Lett. **157B**, 469 (1985).

[7] H. J. Grabosch *et al.* (SKAT Collaboration), Coherent pion production in neutrino and anti-neutrino interactions on nuclei of heavy freon molecules, Z. Phys. C **31**, 203 (1986).

[8] C. Baltay, M. Bregman, D. Caroumbalis, L. D. Chen, M. Hibbs, J. T. Liu, J. Okamitsu, G. Ormazabal, A. C. Schaffer, K. Shastri *et al.*, Evidence for Coherent Neutral Pion Production by High-Energy Neutrinos, Evidence for Coherent Neutral Pion Production by High-energy Neutrinos, Phys. Rev. Lett. **57**, 2629 (1986).

[9] P. Marage *et al.* (BEBC WA59 Collaboration), Coherent single pion production by anti-neutrino charged current interactions and test of PCAC, Z. Phys. C **31**, 191 (1986).

[10] M. Aderholz *et al.* (E632 Collaboration), Coherent Production of $\pi^+\pi^-$ Mesons by Charged Current Interactions of Neutrinos and Anti-Neutrinos on Neon Nuclei at the Tevatron, Phys. Rev. Lett. **63**, 2349 (1989).

[11] P. Marage *et al.* (BEBC WA59 Collaboration), Coherent production of π^+ mesons in ν-neon interactions, Z. Phys. C **43**, 523 (1989).

[12] S. Willocq *et al.* (E632 Collaboration), Coherent production of single pions and rho mesons in charged current interactions of neutrinos and anti-neutrinos on neon nuclei at the Fermilab Tevatron, Phys. Rev. D **47**, 2661 (1993).

[13] M. Hasegawa *et al.* (K2K Collaboration), Search for Coherent Charged Pion Production in Neutrino-Carbon Interactions, Phys. Rev. Lett. **95**, 252301 (2005).

[14] A. A. Aguilar-Arevalo *et al.* (MiniBooNE Collaboration), First observation of coherent π^0 production in neutrino nucleus interactions with $E_\nu < 2$ GeV, Phys. Lett. B **664**, 41 (2008).

[15] K. Hiraide *et al.* (SciBooNE Collaboration), Search for charged current coherent pion production on carbon in a few-GeV neutrino beam, Phys. Rev. D **78**, 112004 (2008).

[16] C. T. Kullenberg *et al.* (NOMAD Collaboration), A measurement of coherent neutral pion production in neutrino neutral current interactions in NOMAD, Phys. Lett. B **682,** 177 (2009).

[17] Y. Kurimoto *et al.* (SciBooNE Collaboration), Improved measurement of neutral current coherent π^0 production on carbon in a few-GeV neutrino beam, Phys. Rev. D **81,** 111102 (2010).

[18] D. Rein and L. M. Sehgal, Coherent π^0 production in neutrino reactions, Nucl. Phys. **B223,** 29 (1983).

[19] S. L. Adler, Tests of the conserved vector current and partially conserved axial-vector current hypotheses in high-energy neutrino reactions, Phys. Rev. **135,** B963 (1964).

[20] D. G. Michael *et al.* (MINOS Collaboration), Observation of Muon Neutrino Disappearance with the MINOS Detectors and the NuMI Neutrino Beam, Phys. Rev. Lett. **97,** 191801 (2006).

[21] A. Bercellie *et al.* (MINERvA Collaboration), Simultaneous measurement of muon neutrino ν_μ charged-current single π^+ production in CH, C, H_2O, Fe, and Pb targets in MINERvA, Phys. Rev. Lett. **131,** 011801 (2023).

[22] R. Acciarri *et al.* (DUNE Collaboration), Long-Baseline Neutrino Facility (LBNF) and deep underground neutrino experiment (DUNE): Conceptual design report, Volume 2: The physics program for DUNE at LBNF, arXiv: 1512.06148.

[23] K. Abe *et al.* (Hyper-Kamiokande Proto- Collaboration), Physics potential of a long-baseline neutrino oscillation experiment using a J-PARC neutrino beam and Hyper-Kamiokande, Prog. Theor. Exp. Phys. **2015,** 053C02 (2015).

[24] A. Higuera *et al.* (MINERvA Collaboration), Measurement of Coherent Production of $\pi^\pm$ in Neutrino and Anti-Neutrino Beams on Carbon from E_ν of 1.5 to 20 GeV, Phys. Rev. Lett. **113,** 261802 (2014).

[25] A. Mislivec *et al.* (MINERvA Collaboration), Measurement of total and differential cross sections of neutrino and antineutrino coherent $\pi^\pm$ production on carbon, Phys. Rev. D **97,** 032014 (2018).

[26] R. Acciarri, C. Adams, J. Asaadi, B. Baller, T. Bolton *et al.* (ArgoNeuT Collaboration), First Measurement of Neutrino and Anti-Neutrino Coherent Charged Pion Production on Argon, Phys. Rev. Lett. **113,** 261801 (2014); **114,** 039901(E) (2015).

[27] K. Abe *et al.* (T2K Collaboration), Measurement of Coherent π^+ Production in Low Energy Neutrino-Carbon Scattering, Phys. Rev. Lett. **117,** 192501 (2016).

[28] S. L. Adler, Adventures in theoretical physics: Selected papers of Stephen L. Adler: Drafts of commentaries, arXiv: hep-ph/0505177.

[29] D. Rein and L. M. Sehgal, PCAC and the deficit of forward muons in π^+ production by neutrinos, Phys. Lett. B **657,** 207 (2007).

[30] R. Ainsworth, P. Adamson, B. C. Brown, D. Capista, K. Hazelwood, I. Kourbanis, D. K. Morris, M. Xiao, and M. J. Yang, High intensity operation using proton stacking in the Fermilab Recycler to deliver 700 kW of 120 GeV proton beam, Phys. Rev. Accel. Beams **23,** 121002 (2020).

[31] P. Adamson, K. Anderson, M. Andrews, R. Andrews, I. Anghel, D. Augustine, A. Aurisano, S. Avvakumov, D. S. Ayres, B. Baller *et al.*, The NuMI neutrino beam, Nucl. Instrum. Methods Phys. Res., Sect. A **806,** 279 (2016).

[32] M. Betancourt *et al.* (MINERvA Collaboration), Direct Measurement of Nuclear Dependence of Charged Current Quasielasticlike Neutrino Interactions using MINERvA, Phys. Rev. Lett. **119,** 082001 (2017).

[33] S. Agostinelli *et al.* (GEANT4 Collaboration), GEANT4—a simulation toolkit, Nucl. Instrum. Methods Phys. Res., Sect. A **506,** 250 (2003).

[34] L. Aliaga *et al.* (MINERvA Collaboration), Neutrino flux predictions for the NuMI beam, Phys. Rev. D **94,** 092005 (2016).

[35] L. Aliaga *et al.* (MINERvA Collaboration), Design, calibration, and performance of the MINERvA detector, Nucl. Instrum. Meth. A **743,** 130 (2014).

[36] I. Ambats *et al.* (MINOS Collaboration), The MINOS detectors technical design report, 10.2172/1861363.

[37] D. G. Michael *et al.* (MINOS Collaboration), The magnetized steel and scintillator calorimeters of the MINOS experiment, Nucl. Instrum. Methods Phys. Res., Sect. A **596,** 190 (2008).

[38] C. Andreopoulos, A. Bell, D. Bhattacharya, F. Cavanna, J. Dobson, S. Dytman, H. Gallagher, P. Guzowski, R. Hatcher, P. Kehayias *et al.*, The GENIE neutrino Monte Carlo generator, Nucl. Instrum. Methods Phys. Res., Sect. A **614,** 87 (2010).

[39] C. Andreopoulos, C. Barry, S. Dytman, H. Gallagher, T. Golan, R. Hatcher, G. Perdue, and J. Yarba, The GENIE neutrino Monte Carlo generator: Physics and user manual, arXiv:1510.05494.

[40] C. H. Llewellyn Smith, Neutrino reactions at accelerator energies, Phys. Rep. **3,** 261 (1972).

[41] A. S. Meyer, M. Betancourt, R. Gran, and R. J. Hill, Deuterium target data for precision neutrino-nucleus cross sections, Phys. Rev. D **93,** 113015 (2016).

[42] J. Nieves, J. E. Amaro, and M. Valverde, Inclusive quasielastic neutrino reactions, Phys. Rev. C **70,** 055503 (2004); **72,** 019902(E) (2005).

[43] J. Nieves, I. Ruiz Simo, and M. J. Vicente Vacas, Inclusive charged-current neutrino-nucleus reactions, Phys. Rev. C **83,** 045501 (2011).

[44] R. Gran, J. Nieves, F. Sanchez, and M. J. Vicente Vacas, Neutrino-nucleus quasi-elastic and 2p2h interactions up to 10 GeV, Phys. Rev. D **88,** 113007 (2013).

[45] J. Schwehr, D. Cherdack, and R. Gran, GENIE implementation of IFIC Valencia model for QE-like 2p2h neutrino-nucleus cross section, arXiv:1601.02038.

[46] P. A. Rodrigues *et al.* (MINERvA Collaboration), Identification of Nuclear Effects in Neutrino-Carbon Interactions at Low Three-Momentum Transfer, Phys. Rev. Lett. **116,** 071802 (2016).

[47] D. Rein and L. M. Sehgal, Neutrino excitation of baryon resonances and single pion production, Ann. Phys. (N.Y.) **133,** 79 (1981).

[48] P. Rodrigues, C. Wilkinson, and K. McFarland, Constraining the GENIE model of neutrino-induced single pion production using reanalyzed bubble chamber data, Eur. Phys. J. C **76,** 474 (2016).

[49] P. Stowell *et al.* (MINERvA Collaboration), Tuning the GENIE pion production model with MINERvA data, Phys. Rev. D **100**, 072005 (2019).

[50] A. Bodek, I. Park, and U. k. Yang, Improved low Q^2 model for neutrino and electron nucleon cross sections in few GeV region, Nucl. Phys. B, Proc. Suppl. **139**, 113 (2005).

[51] D. Ruterbories *et al.* (MINERvA Collaboration), Simultaneous Measurement of Proton and Lepton Kinematics in Quasielasticlike $\nu\mu$-Hydrocarbon Interactions from 2 to 20 GeV, Phys. Rev. Lett. **129**, 021803 (2022).

[52] L. Aliaga *et al.* (MINERvA Collaboration), MINERvA neutrino detector response measured with test beam data, Nucl. Instrum. Methods Phys. Res., Sect. A **789**, 28 (2015).

[53] MINERvA uses a right-handed coordinate system with the y axis pointing upwards and the z axis pointing into the detector parallel to the floor, and almost parallel to the beam plane.

[54] J. Neyman and E. S. Pearson, On the problem of the most efficient tests of statistical hypotheses, Phil. Trans. R. Soc. A **231**, 289 (1933).

[55] See Supplemental Material at http://link.aps.org/supplemental/10.1103/PhysRevLett.131.051801 for background scale factors, cross section tables and additional kinematic variables.

[56] G. D'Agostini, A multidimensional unfolding method based on Bayes' theorem, Nucl. Instrum. Methods Phys. Res., Sect. A **362**, 487 (1995).

[57] J. Tena-Vidal, C. Andreopoulos, A. Ashkenazi, C. Barry, S. Dennis *et al.* (GENIE Collaboration), Neutrino-nucleon cross-section model tuning in GENIE v3, Phys. Rev. D **104**, 072009 (2021).

[58] P. Stowell, C. Wret, C. Wilkinson, L. Pickering *et al.*, NUISANCE: A neutrino cross-section generator tuning and comparison framework, J. Instrum. **12**, P01016 (2017).

[59] C. Berger and L. M. Sehgal, PCAC and coherent pion production by low energy neutrinos, Phys. Rev. D **79**, 053003 (2009).

[60] Diffractive scattering in H was not measured, and no correction is applied for its contribution to the coherent cross section in CH because those events are removed by the vertex energy cut.

[61] K. S. Lackner, Coherent meson production as a test for neutral weak currents of exotic space-time structure, Nucl. Phys. **B153**, 526 (1979).

[62] J. Hufner, Pions interact with nuclei, Phys. Rep. **21**, 1 (1975).

[63] B. Z. Kopeliovich, I. Schmidt, and M. Siddikov, Neutrino-production of single pions: Dipole description, Phys. Rev. D **84**, 033012 (2011).

[64] B. Z. Kopeliovich, I. Schmidt, and M. Siddikov, Diffractive neutrino-production of pions on nuclei: Adler relation within the color-dipole description, Phys. Rev. D **85**, 073003 (2012).

[65] A. A. Belkov and B. Z. Kopeliovich, Adler relation and neutrino production of single hadrons, Sov. J. Nucl. Phys. **46**, 499 (1987), https://inspirehep.net/literature/238754.

[66] M. F. Carneiro *et al.* (MINERvA Collaboration), High-Statistics Measurement of Neutrino Quasielasticlike Scattering at 6 GeV on a Hydrocarbon Target, Phys. Rev. Lett. **124**, 121801 (2020).

[67] E. Valencia *et al.* (MINERvA Collaboration), Constraint of the MINERvA medium energy neutrino flux using neutrino-electron elastic scattering, Phys. Rev. D **100**, 092001 (2019).